Properties of manganese (III) oxide (Mn_2O_3) catalyst for use in Fe-air batteries

Edwine Matlou[1*], *Tshegofatso* Phaahla[1], *Phuti* Ngoepe[1] & *Khomotso* Maenetja[1]

[1]Materials Modelling Centre, University of Limpopo, Private Bag x1106, Sovenga 0727, South Africa

Abstract. Fe-air batteries are promising energy storage devices with high energy density, excellent electrochemical performance, and affordability with low toxicity. However, challenges such as high over-potential, limited cycle life, and side reactions hinder its widespread applications. To address this, we performed density functional theory (DFT) calculations to investigate the structural, thermodynamic, and electronic properties of bulk Mn_2O_3. The calculated lattice parameters for Mn_2O_3 were in good agreement with experimental data with less than 2% difference. Mn_2O_3 is thermodynamically stable, shown by negative $\Delta H°f$ (-821.46 kJ/mol). The electronic band structures and the density of states (DOS) showed that the system has a direct band gap of 0.449 eV, displaying semiconducting behaviour. Thus, the partial density of states (PDOS) identified Mn-d states as the primary contributors to electronic states at E_f, with O-p orbitals participating through hybridization. These findings provide insights into Mn_2O_3's potential as a catalyst in Fe-air batteries.

1 Introduction

The rising global economy and improving living standards have led to a significant increase in energy demand, resulting in a 57.5% rise in global greenhouse gas emissions from fossil fuel use, thereby contributing to climate change [1]. Therefore, advancing modern rechargeable energy storage devices is crucial for creating a more sustainable future [2]. Cleaner energy production has been made possible by the development of alternative energy sources including solar [3], wind [4], and battery technologies [5]. Metal-air batteries have gained attention as a next-generation energy storage solution, delivering a practical specific capacity of 400-1700 Wh/kg [6], which is nearly five times higher than that of traditional lithium-ion batteries (100-200 Wh/kg) [7]. The Fe-air battery (764 Wh/kg) is a standout due to its cost-effectiveness and eco-friendly nature. It is a type of metal-air battery that combines a metallic negative electrode having a low redox potential with air positive electrode. The iron-air battery is composed of three essential components: the iron-based negative electrode, the air-based positive electrode, and an alkaline electrolyte. The theoretical voltage of this system, approximately 1.28 V, arises from the Fe(II)/Fe (0) and Fe(III)/Fe(II) redox reactions at the negative electrode,

* Corresponding author: matlouedwin49@gmail.com

coupled with oxygen reduction at the positive electrode [8]. Unlike zinc-air batteries with a 1083 Wh/kg theoretical specific capacity, Fe-air battery has the added advantage of being less prone to dendrite formation [9]. However, their widespread commercialization is hindered by challenges such as high over-potential between the oxygen evolution reaction (OER) and the oxygen reduction reaction (ORR) and reduces the cycle life-limiting the performance of the Fe-air batteries [10], wherein a substantial amount of energy is lost during the charge-discharge cycle. A key challenge to achieving higher performance is the inherently sluggish kinetics of the ORR, which limits the efficiency and power output of Fe–air batteries by slowing down the cathodic reaction and increasing energy losses [11]. To alleviate these issues, the incorporation of bi-functional electrocatalysts into the air cathode was shown to improve the electrochemical performance and formation of stable discharge products [12]. In this study, we report the structural, thermodynamic and electronic properties of the bulk Mn_2O_3 potential catalyst for use in Fe-air batteries.

2 Materials and methodology

The density functional theory (DFT) [13] code embedded with VASP software [14] was employed to probe into the structural, thermodynamic and electronic properties of Mn2O3 structure within the generalized gradient approximation (GGA) with the Perdew-Burke-Ernzerhof (PBE) exchange-correlation functional [15]. For successful optimization, a planewave energy cut-off of 560 eV and k-point mesh of 4×4×4 with the addition of a Hubbard U parameter of 4 eV to correct self-interaction error in localized d-orbitals (Mn), was found sufficient to fully converge the Mn2O3 bulk structure, ensuring accurate optimization of the lattice parameters.

Thermodynamic stability was assessed by calculating the heats of formation ($\Delta H°f$) of Mn_2O_3 from the total energies of the optimized Mn_2O_3 bulk, elemental Mn in its stable α–Mn phase, and an isolated O_2 molecule. The total density of states (TDOS), partial density of states (PDOS) and band structure were calculated to gain insight into the material's electronic behavior.

3 Results and discussion

3.1 Mechanical and thermodynamic properties

3.1.1 Lattice parameters and heats of formation

Manganese (III) oxide (Mn_2O_3) crystallizes in an orthorhombic crystal system with the Pbca space group (no. 61). In this orthorhombic arrangement, Mn^{3+} ions occupy octahedral coordination sites, where each manganese ion is surrounded by six oxygen atoms, forming slightly distorted MnO_6 octahedral. The oxygen ions occupy general positions and link the Mn-centered octahedral through shared corners and edges, generating a three-dimensional network. Upon full optimization, the structural properties of Mn_2O_3 were successfully determined using DFT calculations, with the computed lattice parameters (a = 9.418 Å, b = 9.423 Å, c = 9.412 Å) closely matching experimental data [16] as shown in Table 1 below. These values confirm the orthorhombic nature of the structure, with a percentage deviation of only 2% from experimental measurements, demonstrating the accuracy of the computational approach.

The large negative heats of formation obtained for Mn_2O_3, both computational (–821.46 kJ·mol^{-1}) and experimental (–961.536 kJ·mol^{-1} [17]), indicate that Mn_2O_3 is highly thermodynamically stable with respect to its constituent elements at standard conditions. A more negative ΔH°f signifies a greater thermodynamic driving force for the compound to form from metallic Mn and O_2 gas, and consequently a lower tendency for decomposition back into those elements. This stability is important in practical applications such as Fe–air batteries, where the cathode material must maintain structural integrity and resist phase decomposition under operating conditions.

Table 1. The theoretical lattice parameters (in Å) and heats of formation (kJ/mol) for Mn_2O_3 bulk structure. The experimental values are referenced for comparison.

Structure		Symmetry	Calculated	Experiment
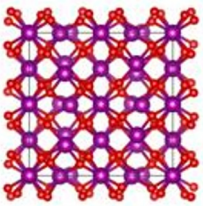	Mn_2O_3	Pbca	a = 9.418 b = 9.423 c = 9.412 α=β=γ=90	a = 9.416 [16] b = 9.423 c =9.405 α=β=γ=90
ΔH°f			-821.46	-961.536 [17]

3.2 Electronic properties

3.2.1 Total density of states (TDOS) and band structure

The density of states (DOS) represents the number of available quantum states at each energy level per unit volume and per unit energy in a system [18]. It describes how electronic states are distributed as a function of energy and indicates how many states are accessible for electrons to occupy at a given energy. In contrast, the band structure of a material illustrates how the allowed electronic energy levels vary with the electron's momentum (wave-vector) within the crystal lattice. It provides detailed insight into both the allowed energy bands and the forbidden energy regions (band gaps).

The band gap reflects the relative position of the valence band maximum (VBM) and the conduction band minimum (CBM) in the electronic structure, representing the energy difference between the highest occupied state in the valence band and the lowest unoccupied state in the conduction band. The magnitude of the band gap directly influences the material's electronic properties: a large band gap corresponds to insulating behaviour, while a smaller band gap permits semiconducting behaviour [19].

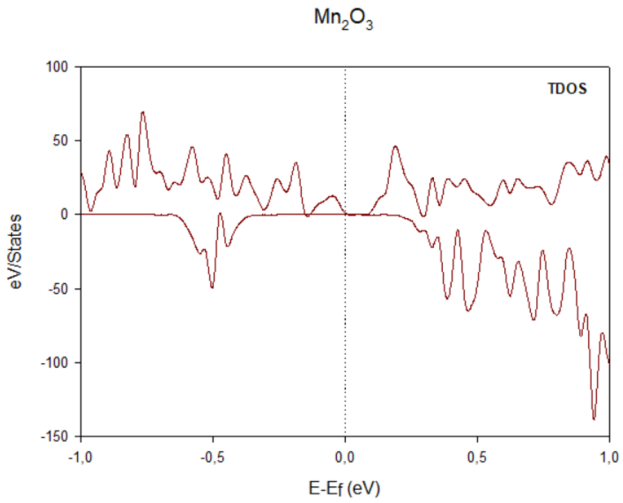

Fig. 1. The spin polarized total density of states for Mn_2O_3 bulk structure.

Figure 1 above shows the spin polarized total density of states (TDOS) for bulk Mn_2O_3 system around the Fermi energy (E_f). The spin-up and spin down channels are asymmetric, consistent with magnetic Mn-3d states. Notably, near the E_f the TDOS is small, indicating semiconducting behaviour. This semiconducting nature arises from the clear depletion of states at the fermi level, where the spin-up and spin down curves both dip to ~0 around 0 eV.

Thus, this dip is attributed to the gap (or a very narrow pseudogap) separating occupied and unoccupied orbitals. A true metal would show finite DOS right at 0 eV. The observed sharp peaks and valleys correspond to localized Mn-3d contributions hybridized with O-2p states. The peaks just below E_f arise mainly from occupied Mn-3d and O-2p bonding states, while those above the Fermi level originate from the unoccupied Mn-3d orbitals. The visual estimate of the gap from TDOS appears to be smaller than experimental values (~1.29 eV) [20].

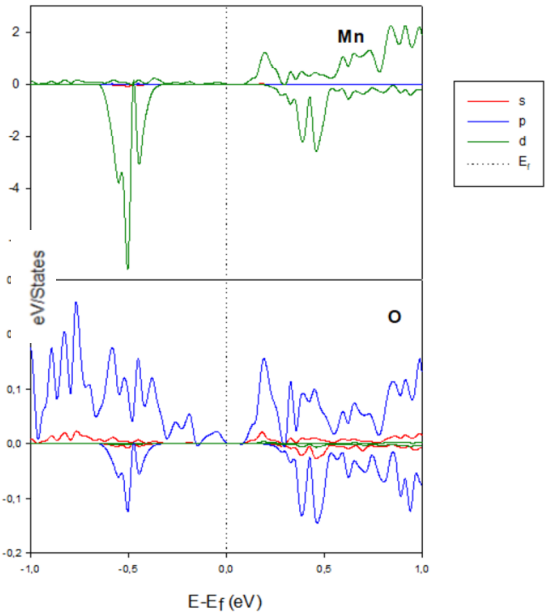

Fig. 2. The spin polarized partial density of states for Mn_2O_3 bulk structure.

The partial density of states (PDOS) in figure 2 above reveal that states near E_f are predominantly contributed by Mn-d orbitals, with minor contributions from O-p orbitals. The Mn-d states exhibit significant intensity both just below and above E_f, implying strong Mn-centered electronic activity around the Fermi level. The hybridization between Mn-d and O-p states, visible in the overlapping energy ranges around E_f, indicates covalent Mn-O bonding interactions. Such hybridization can influence surface reactivity by modifying the adsorption strength of oxygen-containing intermediates.

Below the Fermi level (around -0.5 eV), the PDOS shows a dominant Mn-d contribution with a corresponding O-p feature, suggesting bonding interactions between Mn and O atoms. Above E_f, unoccupied Mn-d states dominate, which could facilitate electron acceptance during ORR. The relatively low contribution from Mn-s and O-s orbitals in this energy range indicates that these states play a negligible role in the surface catalytic behavior.

The band structure in figure 3 is observed to agree with the density of states by confirming that the system is a semiconductor, since there is a direct band gap of 0.449 eV. The reduced gap in Mn_2O_3 suggests higher intrinsic electronic conductivity, which can facilitate faster charge transfer during oxygen reactions.

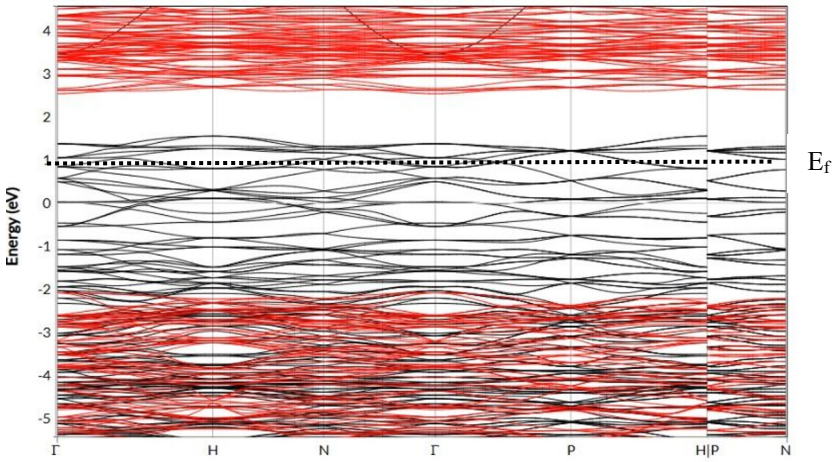

Fig. 3. The band structure for Mn_2O_3 bulk system.

4 Conclusion

This study explored the structural and electronic properties of manganese (III) oxide (Mn_2O_3) as a potential catalyst for Fe–air batteries employing density functional theory (DFT) calculations. The optimized lattice parameters showed excellent agreement with experimental data, and the large negative heats of formation confirmed strong thermodynamic stability. Electronic structure analysis indicated narrow-gap semiconducting behaviour with Mn–d states dominating near the Fermi level and strong Mn–O hybridization, features that may facilitate charge transfer and influence the binding of ORR/OER intermediates. These results establish a solid foundation for subsequent surface and adsorption studies to directly evaluate catalytic activity under battery-relevant conditions.

The computations for this research were performed using resources at the Materials Modelling Centre, University of Limpopo, and the Centre for High Performance Computing (CHPC) in Cape Town. The authors gratefully acknowledge the financial support provided by the South African Department of Science and Innovation (DSI), which also provided open access funding. The data supporting the findings of this study are available from the corresponding author upon reasonable request.

References

[1] Md. A. Siddik, Md. T. Islam, A. K. M. M. Zaman, and Md. M. Hasan, Current Status and Correlation of Fossil Fuels Consumption and Greenhouse Gas Emissions. Int. J. Electr. Electron. Eng. **28**, 103-119 (2021).

[2] M. Asmare, M. Zegeye, and A. Ketema, Advancement of electrically rechargeable metal-air batteries for future mobility. Energy Rep. **11**, 1199-1211 (2024).

[3] R. Prăvălie, I. Sîrodoev, J. Ruiz-Arias, and M. Dumitrașcu, Using renewable (solar) energy as a sustainable management pathway of lands highly sensitive to degradation in Romania. A countrywide analysis based on exploring the geographical and technical solar potentials. Renew. Energy. **193**, 976-990 (2022).

[4] A. G. Olabi et al., Wind energy contribution to the sustainable development goals: case study on London array. Sust. **15**, 4641 (2023).

[5] U.S. Department of Energy, "Energy efficiency and renewable energy," US Government, Department of Energy, Tech. Rep, 2008.

[6] G. Girishkumar, B. McCloskey, A. C. Luntz, S. Swanson, and W. Wilcke, J.Phys, Lithium−Air Battery: Promise and Challenges. Chem. Lett. **1**, 2193-2203 (2010).

[7] M. A. Alemu, A. K. Worku, and M. Z. Getie, Recent advances in electrically rechargeable transition metal-based-air batteries for electric mobility. Inorg. Chem. Commun. **159**, 111742 (2024).

[8] M. Egashira, SECONDARY BATTERIES – METAL-AIR SYSTEMS | Iron–Air (Secondary and Primary), in Encyclopedia of Electrochemical Power Sources, Elsevier, (2009).

[9] S. Trocino, M. Lo Faro, S. C. Zignani, V. Antonucci, and A. S. Aricò, High performance solid-state iron-air rechargeable ceramic battery operating at intermediate temperatures (500–650 °C). Appl. Energy. **233–234**, 386-394 (2019).

[10] S. Narayanan, S. Prakash, A. Manohar, B. Yang, S. Malkhandi, and A. Kinder, Materials challenges and technical approaches for realizing inexpensive and robust iron–air batteries for large-scale energy. Solid State Ion. **216**, 105-109 (2012).

[11] Z. Lu, W. Xu, J. Ma, Y. Li, X. Sun, and L. Jiang, Superaerophilic Carbon-Nanotube-Array Electrode for High-Performance Oxygen Reduction Reaction. Adv. Mater. **28**, 7155-7161 (2016).

[12] Y. Arafat, M. R. Azhar, Y. Zhong, X. Xu, M. O. Tadé, and Z. Shao, A bi-functional air electrode developed from a dual-MOF strategy for high-performance zinc–air batteries. EES Catal. **2**, 968-979 (2024).

[13] A. Moradabadi and P. Kaghazchi, Defect chemistry in cubic Li6.25Al0.25La3Zr2O12 solid electrolyte: A density functional theory study Solid State Ion. **338**, 74-79 (2019).

[14] Z. Liu, Y. Qi, Y. X. Lin, L. Chen, P. Lu, and L. Q. Chen, Interfacial Study on Solid Electrolyte Interphase at Li Metal Anode: Implication for Li Dendrite Growth. J. Electrochem. Soc. **163**, A592-A598 (2016).

[15] P. Perdew, K. Burke, and M. Ernzerhof, Generalized gradient approximation made simple. Phys. Rev. Lett. **77**, 3865 (1996).

[16] S. Geller, Structure and Magnetic Ordering of α-Mn_2O_3, $(Mn_{0.983}Fe_{0.017})_2O_3$, and $(Mn_{0.37}Fe_{0.63})_2O_3$. Struct. Dyn. **27**, 821-828 (1971).

[17] K. T. Jacob, A. Kumar, G. Rajitha, Y. Waseda, Thermodynamic data for Mn_3O_4, Mn_2O_3 and MnO_2. High Temp. Mater. Process. **30**, 459–472 (2011).

[18] R. Dick, Advanced quantum mechanics: Materials and photons (Springer, New York, 2012)

[19] Y. Ling et al., Mapping between density of states and energy band gap for bismuth-based semiconductors via machine learning prediction. Fuel. **331**, 125925 (2023).

[20] H. Rahaman et al., Fabrication of Mn2O3 nanorods: an efficient catalyst for selective transformation of alcohols to aldehydes. RSC Adv. **5**, 33923-33929 (2015).